NPG Asia Materials (2012) 4, e12; doi:10.1038/am.2012.22

www.nature.com/am

ORIGINAL ARTICLE

Significant increase in the water dispersibility of zinc phthalocyanine nanowires and applications in cancer phototherapy

Hye Kyung Moon[1], Minhyeok Son[1], Ji Eun Park[1], Seok Min Yoon[1], Sang Ho Lee[2] and Hee Cheul Choi[1]

The phototherapy is one of the widely accepted noninvasive clinical methodologies to eradicate cancer cells owing to its minimal side effects and high selectivity to the light of specific wavelength. As represented by photodynamic (PD) and photothermal (PT) therapy, the phototherapy requires light and photosensitizer to generate reactive oxygen species and heat, respectively. Zinc phthalocyanine (ZnPc) is one of the promising photosensitizers as it has a strong absorption cross-section in the spectral range of 650–900 nm that guarantees maximum tissue penetration. One critical issue in using Pc molecule, including ZnPc as a biocompatible sensitizer is the poor water solubility. To increase water solubility, various chemical modifications inducing hydrophilicity have been widely attempted to introduce various functional groups in the ZnPc backbone. We report that ZnPc nanowires (NWs) directly grown from ZnPc powder by vaporization–condensation–recrystallization process show surprisingly increased water dispersibility without any functionalization. The ZnPc NW solution exhibits highly efficient dual PD and PT effects upon the irradiation of near infrared (808 nm) laser. The dual phototherapeutic effect of ZnPc NW is proven to enhance cytotoxic efficiency according to both *in vitro* and *in vivo* experimental results.
NPG Asia Materials (2012) **4,** e12; doi:10.1038/am.2012.22; published online 13 April 2012

Keywords: nanowire; photosensitizer; phototherapy; Zinc phthalocyanine

INTRODUCTION

Phototherapy, represented by photodynamic therapy (PDT) and photothermal therapy (PTT), is an advanced modality for the treatment of malignant tumors as it is widely used for clinical cancer treatments. PDT selectively destroys neoplastic lesions using cytotoxic reactive oxygen species (ROS) generated by light activation of the photosensitizer.[1,2] One of the crucial factors determining the PDT efficacy is the photochemical and photophysical properties of the photosensitizer.[3,4] Currently, four main classes of photosensitizer, such as porphyrin derivatives, chlorins, porphycenes, and phthalocyanines (Pcs), have been approved by the U.S. Food and Drug Administration (FDA) for clinical applications against cancer.[5,6] Among these, metallo-phthalocyanine has attracted considerable interest, having a photodynamic (PD) property that can be readily tuned by the type of central metal ion and the functional groups introduced as a Pc ring substituent. Zinc phthalocyanine (ZnPc) is known to exhibit a high PD effect as it possesses a diamagnetic Zn(II) central metal ion whose *d* shell is fully occupied, by which the yield of triplet excited state with long lifetime essential for the generation of ROS becomes high.[7] Moreover, ZnPc has a large absorption cross-section of light at the tissue-penetrating spectral range of 650–900 nm.[7,8]

The biggest hurdle for most photosensitizers, including ZnPc, for PDT is the low physiological acceptance level owing to their high hydrophobic characteristics responsible for the poor solubility in a bodily fluid. To overcome this problem, ZnPc derivatives, such as tetrasulfonated ZnPc ($ZnPcS_4$),[9] [1,2,3,4-tetrakis(α/β-D-galactopyranos-6-yl)-phthalocyaninato]zinc,[10] tetra- and octa-triethyleneoxysulfonyl substituted ZnPc,[11] have been designed to increase the water solubility. Various delivery vehicles including liposome,[12] emulsion[13] and nanoparticles[14] have also been developed to transport water-insoluble photosensitizers to targets. However, these approaches require multiple and complex chemical functionalization steps, during which the photoactivity could be reduced by destroying the original electronic conjugation system of the photosensitizer.[15] Another challenging issue is the realization of a photosensitizer that exhibits both PD and photothermal (PT) effects simultaneously to conduct dual synergistic phototherapy, which is rarely found from a single photosensitizer.

[1]Department of Chemistry and Division of Advanced Materials Science, Pohang University of Science and Technology (POSTECH), Pohang, Korea and [2]Department of Surgery, Kosin University College of Medicine, Busan, Korea
Correspondence: Professor HC Choi, Department of Chemistry and Division of Advanced Materials Science, Pohang University of Science and Technology (POSTECH), San 31, Hyoja-Dong, Nam-Gu, Pohang 790-784, Korea.
E-mail: choihc@postech.edu
or Professor SH Lee, Department of Surgery, Kosin University College of Medicine, 34 Amnam-Dong, Seo-Gu, Busan 602-702, Korea.
E-mail: gslsh@kosinmed.or.kr
Received 21 October 2011; revised 7 February 2012; accepted 4 March 2012

Herein, we report that water dispersibility of ZnPc significantly increases as ZnPc molecules are self-crystallized into one-dimensional nanowire (NW) crystals, even without any special functional groups introduced. Upon irradiation with near infrared (NIR, $\lambda = 808$ nm) laser light, the ZnPc NWs exhibit a PD property. Moreover, the ZnPc NWs show a PT property that is known to be absent from ZnPc powder (PW). The highly efficient dual PD and PT properties are examined from both *in vitro* and *in vivo* experiments. Such a dual modality from a single molecule has significant advantages for the development of multifunctional molecular systems to grant a greater therapeutic efficacy.

MATERIALS AND METHODS

Synthesis of ZnPc NWs

ZnPc PW (0.05 g, Sigma-Aldrich, St Louis, MO, USA) was loaded in a ceramic boat, which was located at the center of a quartz tube placed in an electrical heating furnace system. A Si(100) substrate was placed at the end region of the furnace. Before the reaction, the quartz tube was flushed with Ar gas at a flow rate of 800 sccm for 5 min to remove trapped ambient gases and then heated up to 550 °C under steady Ar flow. The reaction was maintained for 40 min for ZnPc NW growth and then the sample was cooled to room temperature under Ar flow.

Characterization of ZnPc NWs

Thermogravimetric measurement was carried out using a thermogravimetry analyzer (TG-2171, Cahn Instrument Inc., Cerritos, CA, USA). ZnPc PW (5 mg) was loaded and heated from room temperature to 1000 °C at a rate of 4 °C per min under Ar atmosphere. The morphology, chemical elements and diffraction patterns were analyzed by scanning electron microscopy (SEM, JSM-7410F, JEOL) and transmission electron microscopy (TEM, JEM 2100F, JEOL, Tokyo, Japan). Au was sputtered on ZnPc NWs for SEM measurement. Samples for TEM measurement were prepared by dropping an aqueous solution of ZnPc NWs onto a carbon film-coated Cu grid. X-ray diffraction patterns were obtained using an X-ray diffractometer (XRD, D/MAX-2500/PC, RIGAKU, The Woodlands, TX, USA). For Fourier-transformed infrared (FT-IR) spectroscopy, KBr pellets of ZnPc PW and ZnPc NWs were prepared, and the FT-IR spectra were obtained using an FT-IR spectrophotometer (VERTEX 70, Bruker Optics, Ettlingen, Germany). The integrity of ZnPc NWs was characterized by fast atom bombardment-mass spectrometry (FAB-MS, JMS 700 high-resolution mass spectrometer equipped with FAB ionization, JEOL) and ^{1}H nuclear magnetic resonance (NMR, DMSO-d_6, FT-300 MHz Bruker Aspect 3000). The results of mass spectrum and NMR spectrum were shown as: MS (*m*/*z* calculated, 576.079 [M$^+$]; found, 576.2 [M$^+$]), ^{1}H NMR (ZnPc PW: δ 9.445–9.473 (dd, $J_1 = 5.6$, $J_2 = 3$, 8H ArH); δ 8.274–8.302 (dd, $J_1 = 5.6$, $J_2 = 3$, 8H ArH), ZnPc NW: δ 9.445–9.474 (dd, $J_1 = 5.7$, $J_2 = 3$, 8H ArH); δ 8.285–8.314 (dd, $J_1 = 5.7$, $J_2 = 3$, 8H ArH)).

Preparation and characterization of ZnPc NWs aqueous solution

A ZnPc NWs solution was prepared by adding ZnPc NWs collected from Si substrates into water, followed by sonication for various times in a bath sonicator (UC-10, JEIOTECH, Deajeon, Korea). The final solution was transferred for the measurement of optical absorbance using a UV-vis spectrometer (Agilent 8453 spectrophotometer, Agilent, Santa Clara, CA, USA). The concentration of ZnPc NW solution was determined by measurement of optical absorbance at 219 nm. The calibration curve was made by measuring the optical absorbance of a sequentially diluted solution at 219 nm. The hydrodynamic sizes of ZnPc NW and PW were measured by dynamic light scattering (Malvern Zetasizer Z, Worcestershire, UK).

Investigation of the water-dispersion of ZnPc NWs

ZnPc NWs (0.5 mg) were solubilized in 2 ml dimethylformamide (DMF), and water was added to make a mixture solution at various ratios. The mixture solution was examined for the shift of the Soret band by UV-vis spectroscopy. X-ray photoelectron spectra (XPS) were acquired from the 8A1 beamline of the synchrotron facility at Pohang Accelerator Laboratory, POSTECH. The photon energy was 630 eV.

ROS detection of ZnPc NWs aqueous solution

The generation of ROS was monitored by Image-iT LIVE Reactive Oxygen Species Kit based on H_2DCFDA (Molecular Probes/Invitrogen, Eugene, OR, USA), following the manufacturer's protocol. Pre-seeded KB cells were incubated with ZnPc NW solution (120 mg l^{-1}) for 18 h at 37 °C with 5% CO_2. After washing the cells thoroughly with phosphate buffer saline (PBS), the cells were irradiated with an 808 nm laser. H_2DCFDA (10 μM) was added to the cells and were incubated at 37 °C for 30 min. H_2DCFDA is a fluorogenic marker for ROS, which permeates live cells and is deacetylated by intracellular esterases. In the presence of ROS, the reduced fluorescein compound is oxidized and emits bright green fluorescence. Fluorescence intensity was measured at 529 nm using a fluorescence spectrometer (Cary Eclipse, Varian, Mulgrave, VIC, Australia).

Examination for PT effect of ZnPc NWs aqueous solution

The ZnPc NW solution and zinc phthalocyanine tetrasulfonate ($ZnPcS_4$) solutions at various concentrations (60, 80, 120 mg l^{-1}) were irradiated using a 660/808 nm laser (diode laser, JENOPTIK unique-mode GmbH, Jena, Thuringia, Germany) at 3 W cm^{-2}. The temperature of each solution was measured with a thermocouple connected temperature controller (Hanyoung, Seoul, Korea) at 20-s intervals for a total of 3 min. Three sets per each solution were measured.

Observation of intracellular internalization of ZnPc NWs

As ZnPc shows characteristic Raman bands at 1336, 1506 cm^{-1} corresponding to pyrrole stretching modes, the intracellular internalization of ZnPc NWs was directly identified by confocal Raman spectroscopy. Human epidermoid mouth carcinoma KB cells were cultured in RPMI 1640 medium supplemented with 10% fetal bovine serum and 1% penicillin/streptomycin (all reagents from Hyclone, Logan, UT, USA) at 37 °C in a humidified atmosphere with 5% CO_2. The KB cells were seeded on a glass cover slip in 24-well plates for 18 h at a density of 1×10^5cells per well in 1 ml of medium. The medium was replaced with fresh media and the cells were incubated with 50 mg l^{-1} ZnPc NW solution for 12 h at 37 °C under 5% CO_2 atmosphere. After incubation, the cells were thoroughly rinsed with PBS, then a cell-seeded cover slip was placed on a glass slide for the measurements. The pyrrole stretching band was measured using a Raman spectrometer (laser excitation wavelength of 532 nm, 3 mW power, 100 × objective, 0.3 s integration time, confocal mode, Alpha 300R, Witec, Ulm, Germany). Raman mapping images were collected at 2-μm intervals.

In vitro antitumor effect of ZnPc NWs aqueous solution

Pre-incubated human KB cells (0.5×10^5 cells ml^{-1}) were incubated with ZnPc NW solution (120 mg l^{-1}) for 18 h at 37 °C with 5% CO_2. After incubation, cells were rinsed with PBS followed by irradiation with an 808 nm laser at 3 W cm^{-2} for 5 min. Trypan blue was used to stain the dead cells. Cell viability was determined by CellTiter A96 (Promega, Fitchburg, WI, USA) assay. Each cell samples were treated with tetrazolium compound (3-(4,5-dimethylthiazol-2-yl)-5-(3-carboxymethoxyphenyl)-2-(4-sulfophenyl)-2H-tetrazolium, inner salt; MTS) and electron coupling reagent (phenazine methosulfate; PMS) and incubated for 2 h at 37 °C with 5% CO_2. Absorbance at 490 nm was measured to determine the concentration of formazan, which was bioreduced from MTS by metabolically active and viable cells.

In vivo antitumor effect of ZnPc NWs aqueous solution

The KB cells (1×10^7 cells) were inoculated into the back of male BALB/c mice (n = 4, 5-to 6-week-old). When the tumor volume reached approximately 70 mm^3, the mice were intratumorally injected with ZnPc NW solution (100 μl, 120 mg l^{-1}) and immediately irradiated with an 808 nm laser (3 W cm^{-2}, 3 min) under ether anesthesia. The tumor size was measured every 3 days. All procedures for *in vivo* experiments were performed in accordance with the Pohang University of Science and Technology guidelines on animal care and use.

Histological assessment of tumor tissue

Mice were euthanized 24 h after all treatment, and tumor tissues of each group were resected and fixed overnight in 4% paraformaldehyde solution. Tumor tissues were then embedded in paraffin after tissue processing. Paraffin sections were mounted on a glass slide for histological assessment with hematoxylin

and eosin staining, and with terminal deoxynucleotidyl transferase biotin-dUTP nick-end labeling (TUNEL assay, Calbiochem, San Diego, CA, USA) to detect apoptotic or necrotic cells.

RESULTS AND DISCUSSION

The ZnPc NWs were synthesized by the vaporization–condensation–recrystallization (VCR) process using ZnPc PW as a precursor.[16,17,18,19] During the reaction, ZnPc PW placed at the center of a tube-type heating furnace was vaporized at 550 °C, and ZnPc vapors were delivered by Ar gas downstream where a small piece of Si wafer was located (Figure 1a). The ZnPc vapors were condensed on the Si wafer as the substrate temperature was naturally lowered to 180 °C, at which one-dimensional ZnPc NWs grow. The overall reaction time was 40 min, and the vaporization of ZnPc PW at 550 °C was confirmed by thermogravimetric analysis (Supplementary Figure S1). A representative SEM image of the as-grown ZnPc NWs is shown in Figure 1b. The diameter and length of ZnPc NW ranges from 50 to 100 nm, and 1 to 10 μm, respectively.

The crystal structure of ZnPc NW was characterized by X-ray powder diffraction (XRD) and high-resolution transmission electron microscopy (HR-TEM) with selected area electron diffraction (SAED) data. The XRD results reveal that ZnPc NW has an α-form, whereas the original ZnPc PW has a β-form according to the JC-PDS cards No. 21-1986 and 39-1882. One of the characteristic XRD peaks of ZnPc is the (200) peak. While the β-form ZnPc PW shows $d_{(200)} = 7.24$ Å (at $2\theta = 12.22^{\circ}$), the α-ZnPc NW shows $d_{(200)} = 12.6$ Å (at $2\theta = 7.01^{\circ}$), which agrees well with previously reported values from α-ZnPc bulk crystal and thin film[20,21,22,23] (Figures 1c and d).[24] The FT-IR spectroscopy results further confirm the genuineness of the α-form of ZnPc NW as it displays a fingerprint-bending mode of C–H at 724 cm^{-1} together with the vibrational mode of the center cyclic ring at 773 cm^{-1} (Supplementary Figure S2).[25,26] Note that ZnPc NW samples are collected from multiple reaction batches for the PW XRD measurements.

The HR-TEM images shown in Figures 1e and f clarify that ZnPc NW has well-defined crystalline lattices parallel to the growth direction. The single crystallinity is confirmed from a SAED pattern that exhibits individual diffraction spots (inset in Figure 1e). The (002) lattice spacing of 1.14 nm (Figure 1f) agrees well with the XRD result ($d_{(002)} = 11.5$ Å at $2\theta = 7.66^{\circ}$). The individual lattice lines ((200)

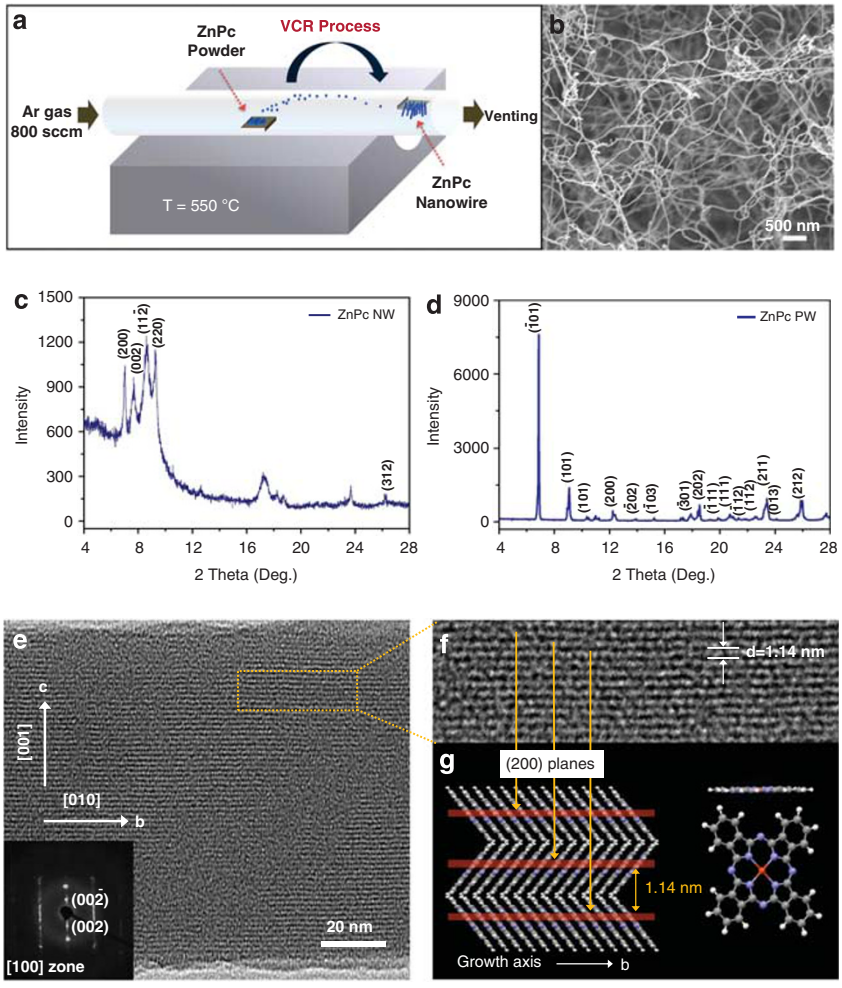

Figure 1 Morphology and structure of ZnPc NW. (**a**) Schematic view of the VCR process growing ZnPc NWs. (**b**) Representative SEM image of ZnPc NWs grown at 550 °C for 50 min by the VCR process. (**c, d**) XRD patterns of ZnPc (α-form) collected from Si(100) substrate, and ZnPc PW (β-form), respectively. (**e**) High resolution TEM image of an isolated single ZnPc NW grown along the [010] direction. (Inset) SAED pattern of the ZnPc NW with [100] projection. (**f**) Magnified view of the yellow outlined box in (**e**). The interplanar spacing of lattice image is about 1.14 nm. (**g**) Schematic view of the crystal structure of ZnPc NW in projection along the a-axis. (Left) Zinc planes are highlighted in red, corresponding to the array of Zn(II) ion in NW. (Right) Molecular structure of ZnPc.

planes along the [100] direction) correspond to linear Zn metal ion arrays as depicted by the red lines in the scheme (Figure 1g). The growth of ZnPc NW follows the direction of self-assembly of ZnPc molecules (along the [010] direction) via π–π stacking, so (200) planes are parallel to the growth direction.[21,27] Indeed, when as-grown ZnPc NWs on a Si substrate are examined, only a single XRD peak from (200) planes appears because most of the ZnPc NWs prefer to lay down on the substrate with (200) planes parallel to the substrate (Supplementary Figure S3). The structure of our ZnPc NW is closely comparable to the previously reported CuPc nanowire.[28]

The preservation of molecular structure of ZnPc in ZnPc NW without any skeletal destruction during the VCR process was confirmed by mass spectroscopy and nuclear magnetic resonance (NMR) spectroscopy. The mass spectra display basically identical chemical compositions for both ZnPc NW and PW as the intense peak at 576.2 *m*/*z*, corresponding to the exact mass of ZnPc (576.079 *m*/*z*), appears from both samples (Supplementary Figure S4). The proton (^{1}H) NMR spectrum of the ZnPc NW further proves that the ZnPc NW contains pure ZnPc without any structural change (Supplementary Figure S5).[29]

The as-grown ZnPc NW disperses well in water with mechanical agitation by sonication (Figure 2a top row). The degree of dispersion of ZnPc NW in water gradually increases as a function of sonication time, which is easily noticed by the color change of the solution from transparent pale blue to dark blue. The successive change in length of ZnPc NW upon sonication that is responsible for the increased water dispersibility is visualized by TEM images (Figure 2a middle row). After sonication for 40 min, most of the ZnPc NWs become nanoparticulates having truncated structures that range from 60 to 90 nm (Figure 2a middle row, Supplementary Figure S6). Note that ZnPc NWs ranging from 50 to 100 nm are still present but at low concentration (inset of third TEM image in Figure 2a). The ZnPc NW aqueous solution is highly stable at room temperature as it stays for over three months without any aggregation. The ZnPc PW sonicated in water, on the other hand, precipitates in a short period of time (Figure 2b). The maximum concentration of the ZnPc NW solution ($\sim$120 mg l^{-1}) is eight times higher than that of the ZnPc PW solution ($\sim$16 mg l^{-1}).

The dispersion of ZnPc NW in water should involve the preferred adsorption of water molecules to ZnPc NW. The preferred interaction of water on ZnPc NW over ZnPc PW was confirmed by Fourier transformed infrared (FTIR) spectroscopy and X-ray photoelectron spectroscopy (XPS) (Supplementary Figure S6). Upon exposure of both samples in air (humidity = 30%) for 2 h, ZnPc NW shows the O-H vibrational band from the water molecule at 3600–3300 cm^{-1}, which is absent for ZnPc PW (Supplementary Figure S7a).[30] The XPS survey spectra data also exhibits the O1s peak at 533 eV corresponding to the O in water[31,32] only from ZnPc NW. The O1s peak disappears when the sample is vacuum annealed (Supplementary Figure S7b).

The preferred adsorption of water to ZnPc NW occurs through hydrogen bonding of water to the N atoms in ZnPc and coordination of water to the Zn(II) ion in ZnPc. Although the hydrogen bonding of water to N atoms in ZnPc is easily agreed, the coordination of water to Zn(II) ions still needs to be confirmed. Therefore, the coordination power of water molecules to the central Zn(II) ion was examined by adding water into a DMF solution of ZnPc NW at various volume ratios. The UV-vis spectrum of pure ZnPc NW/DMF solution shows characteristic Soret and Q bands at 343 nm and 669 nm, respectively. Upon increase of water fraction, the Soret band gradually shifts to higher energy (up to 330 nm), and the solution color changes from green to blue (Supplementary Figure S8). The blue shift of the Soret band implies that DMF molecules pre-coordinated to the Zn(II) ion are replaced by water molecules that have stronger coordination power.[33]

Considering that both hydrogen bonding and coordination of water to Zn(II) ion interactions are equally applicable to both ZnPc PW and NWs, there must be another critical factor that induces higher dispersibility of ZnPc NW over ZnPc PW, and it is the crystal structure. As shown in Figure 2c, all of the hydrogen bonding and water coordination sites are freely available in α-form ZnPc NW. On

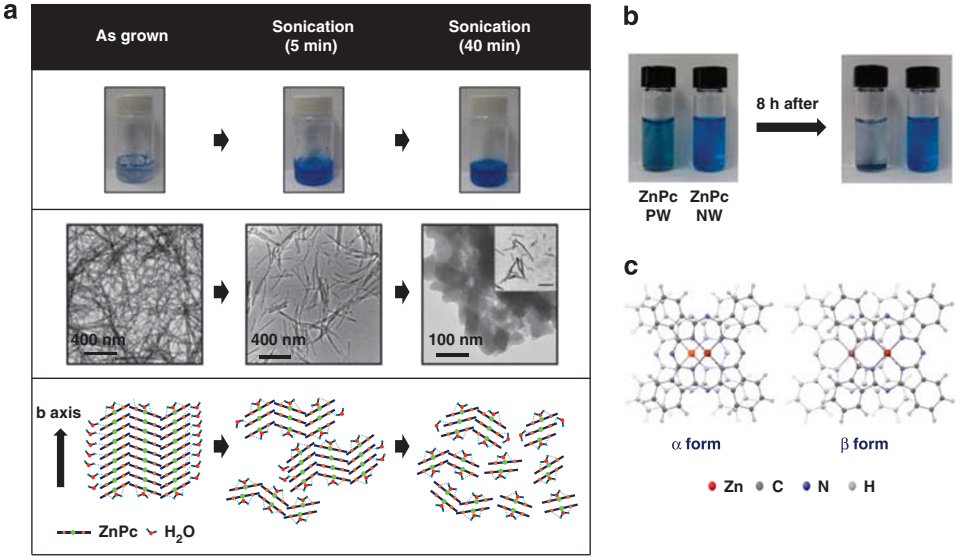

Figure 2 Increased water-solubility of ZnPc NW. (**a**) Dispersion of ZnPc NW in water and the effect of sonication. (Top row) Photographs of ZnPc NWs dispersed in water. (Middle row) TEM images of ZnPc NWs. The ZnPc NWs become shortened during sonication, leading to truncated structures. (Inset of third image) Shortened ZnPc NWs ranging from 50 to 100 nm are sparsely distributed in solution. The scale bar is 400 nm. (Bottom row) Schematic representation of the increased chance of an interaction between water and the ZnPc unit with longer sonication time. The blue dashed lines indicate the hydrogen bonding between hydrogen atoms of water molecule and nitrogen atoms of ZnPc. (**b**) Photographs showing the stability of ZnPc PW and ZnPc NW in water. (**c**) Superposition of ZnPc molecules along the b axis in α-form and β-form polymorphic structures.

the other hand, all Zn(II) ions in β-form PW are pre-coordinated to the framework nitrogen atoms of neighboring ZnPcs, resulting in the loss of both Zn(II) and N interaction sites. Note that this is the main reason for the high stability of β-ZnPc PW. To further prove the effect of crystal structure on the water dispersibility of ZnPc NW and ZnPc PW, we performed control experiments to compare water dispersibilities of ZnPc NW and ZnPc PW that have similar sizes. If the crystal structure has nothing to do with the increased dispersibility of ZnPc NW, both samples should show similar hydrodynamic sizes in water with similar dispersity levels. The hydrodynamic sizes of both dispersed solutions measured by dynamic light scattering right after the sonication are quite similar as the data shows 85.99 nm for ZnPc NW and 89.80 nm for ZnPc PW (Supplementary Figure S9). However, ZnPc PWs measured after 1 h shows a very high polydispersity index value (0.918) due to their aggregation and precipitation. On the contrary, ZnPc NWs are still stable showing a similar size distribution. These results clearly prove that the increased water dispersibility of ZnPc NW arises from the fundamental difference of the polymorphic structure rather than just size.

Meanwhile, hydrogen bonding seems to have a more important role for the dispersibility increase compared with the water coordination to Zn(II), as metal-free phthalocyanine NWs also show a greatly enhanced water solubility (Supplementary Figure S10).

The photoeffect of highly water-dispersible ZnPc NW was examined for the application of cancer phototherapy. Metallo-phthalocyanine generates either ROS or thermal energy upon light illumination in the NIR region depending on the electronic configuration of the central metal. When a central metal possesses d^0 or d^{10} (closed shell, like Zn(II)) electronic configuration, the triplet excited state has a long lifetime sufficient to be involved in the generation of ROS (PD effect). On the other hand, metallo-phthalocyanine having central metals of which the *d* orbitals are not completely occupied (open shell, like Ni(II), Co(II), and so forth) shows low PD effect, but rather exhibits fast conversion of excited electronic energy to the vibrational mode, resulting in a PT effect.[34] Because the required conditions of the electronic energy states of photosensitizers for PD and PT effects mutually conflict, it is difficult to realize photosensitizers that exhibit both photoeffects simultaneously. To enable such a dual phototherapy, composites containing two components generating PD and PT effects have been suggested. Examples include a ZnPc-encapsulated carbon nanohorn[35] and an indocyanine green-conjugated gold nanorod.[36]

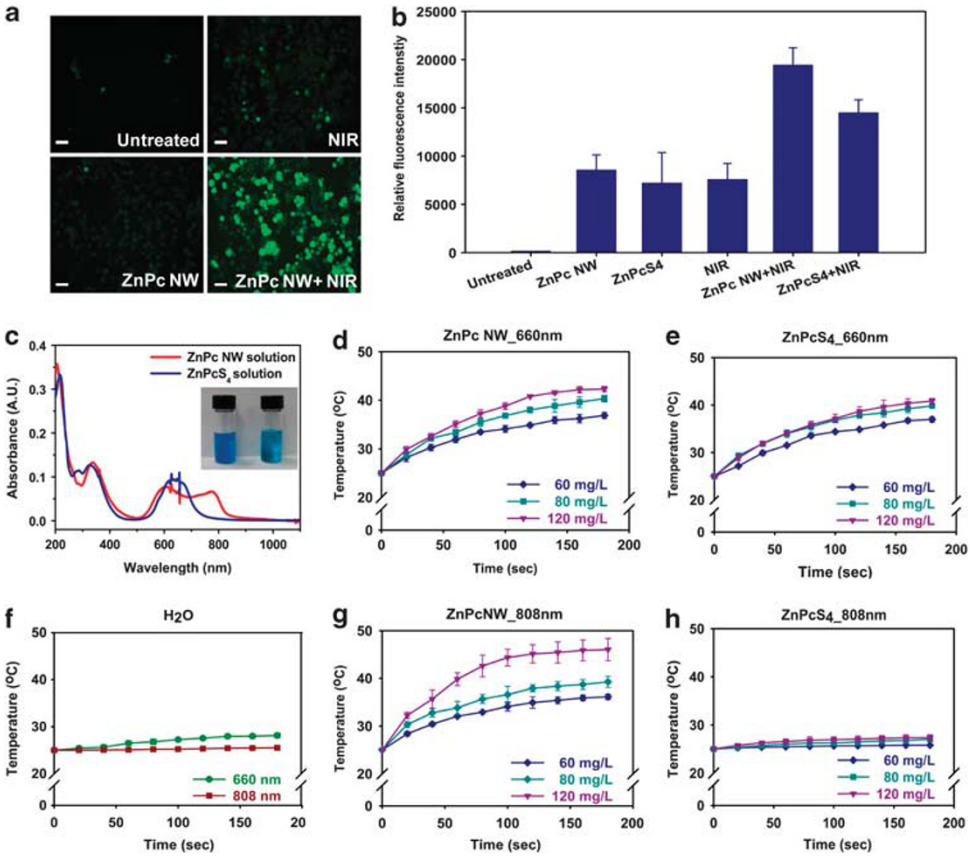

Figure 3 Dual photoeffect of ZnPc NW. (**a**) Fluorescence microscopy images of KB cells to detect oxidative stress using Image-iT LIVE Reactive Oxygen Species (ROS) Kit. (Top left) KB cells untreated, (top right) irradiated with NIR (808 nm, 3 W cm^{-2}), (bottom left) treated with ZnPc NW solution (120 mg l^{-1}), (bottom right) treated with ZnPc NW solution (120 mg l^{-1}) followed by irradiation with NIR (808 nm, 3 W cm^{-2}). The cells showing green fluorescence color represent oxidatively stressed cells affected with ROS. (**b**) Relative fluorescence intensity of each group. Data are expressed as mean ± s.d. (n = 3, triplicate). (**c**) UV-vis spectra of ZnPc NW solution (red line) and $ZnPcS_4$ solution (blue line). High absorptions of ZnPc NW solution (at 600, 800 nm) and $ZnPcS_4$ solution (at 630 nm) in the NIR region are observed. (Inset) A photo of ZnPc NW solution (blue, left) and $ZnPcS_4$ solution (aqua green, right). (**d, e**) Temperature changes of ZnPc NW and $ZnPcS_4$ in water at various concentrations, respectively, upon NIR irradiation (660 nm, 3 W cm^{-2}). (**f**) Temperature changes of pure water upon NIR irradiation (660 nm and 808 nm, 3 W cm^{-2}) for 3 min. (**g, h**) Temperature changes of ZnPc NW and $ZnPcS_4$ in water at various concentrations, respectively, upon NIR irradiation (808 nm, 3 W cm^{-2}) for 3 min. Data are shown as mean ± s.d. (n = 3, triplicate).

Interestingly, the ZnPc NW shows both PD and PT effects upon NIR illumination. The PD activity of ZnPc NW is proven by detecting ROS generated from human epidermoid mouth carcinoma KB cells containing ZnPc NWs upon illumination with NIR ($\lambda = 808$ nm) laser light. The ROS production was assessed using Image-iT LIVE Reactive Oxygen Species Kit (Molecular Probes/Invitrogen).[37] This assay is based on 5- (and 6-)-carboxy-2′7′-dichlorodihydrofluorescein diacetate (carboxy-H_2DCFDA) as a fluorogenic marker for ROS permeated viable cells, and deacetylated by nonspecific intracellular esterase. In the presence of ROS, the reduced carboxy-H_2DCFDA is supposed to be oxidized to emit bright green fluorescence. Therefore, the oxidatively stressed cells by ROS could be recognized by green fluorescence. To compare the effect of ZnPc NW, commercially available $ZnPcS_4$ specially designed to increase water solubility, was tested. As shown in Figures 3a and b, untreated cells, ZnPc NW-treated cells, $ZnPcS_4$-treated cells, and NIR-treated cells show negligible production of ROS. However, ZnPc NW and NIR-treated cells show substantially high green fluorescence intensity. These results clarify that ZnPc NW excited with NIR is responsible for the generation of ROS.

The PT property was then examined by monitoring temperature changes of aqueous ZnPc NW solutions (60, 80, 120 mg l^{-1}) upon light illumination at two different wavelengths (λ) of 660 nm, at which highest absorption occurs, and 808 nm, at which most biological systems become transparent,[38] at the power of 3 W/cm^2. The temperatures of both ZnPc NW and $ZnPcS_4$ solutions increase upon illumination of light ($\lambda = 660$ nm) from room temperature to about 40 °C, which is proportional to the concentration (Figures 3d and e). When 808 nm laser irradiation is used, however, only ZnPc NW solution (120 mg l^{-1}) shows temperature increase up to 46 °C (Figure 3g), whereas pure water and $ZnPcS_4$ solution show negligible temperature changes (Figures 3f–h). Note that there is no photobleaching effect during irradiation for 10 min (Supplementary Figure S11).

The emergence of an unprecedented PT property from ZnPc NW seems to be attributed to the change of electronic energy state of ZnPc upon its self-assembly via π–π stacking. As briefly mentioned, monomeric of ZnPc has PD activity due to its long-lived triplet states. However, stacking of ZnPc molecules via π–π interaction causes transfer of the triplet excitation energy, resulting in a shortened triplet state lifetime together with an increased probability of non-radiative relaxation. This then leads to thermal energy release, which is known as long-range migration of triplet excitation, resulting in triplet–triplet annihilation.[39] Note that the Q-band broadening in ZnPc NW is also attributed to π–π interactions among Pc rings (Figure 3c).

The ZnPc NW solution was then examined for cellular uptake and synergic phototherapy of cancer. The ZnPc NW solution was treated with KB cells to examine its cellular uptake. Confocal microRaman spectroscopy was used to track ZnPc NW in the cell using both spectroscopy and imaging modes. Figure 4a shows characteristic Raman spectra of as-grown ZnPc NW and its aqueous solution. Both Raman spectra exhibit distinct pyrrole stretching bands at 1336 and 1506 cm^{-1}, which are used as reference signals.[40] After incubating KB

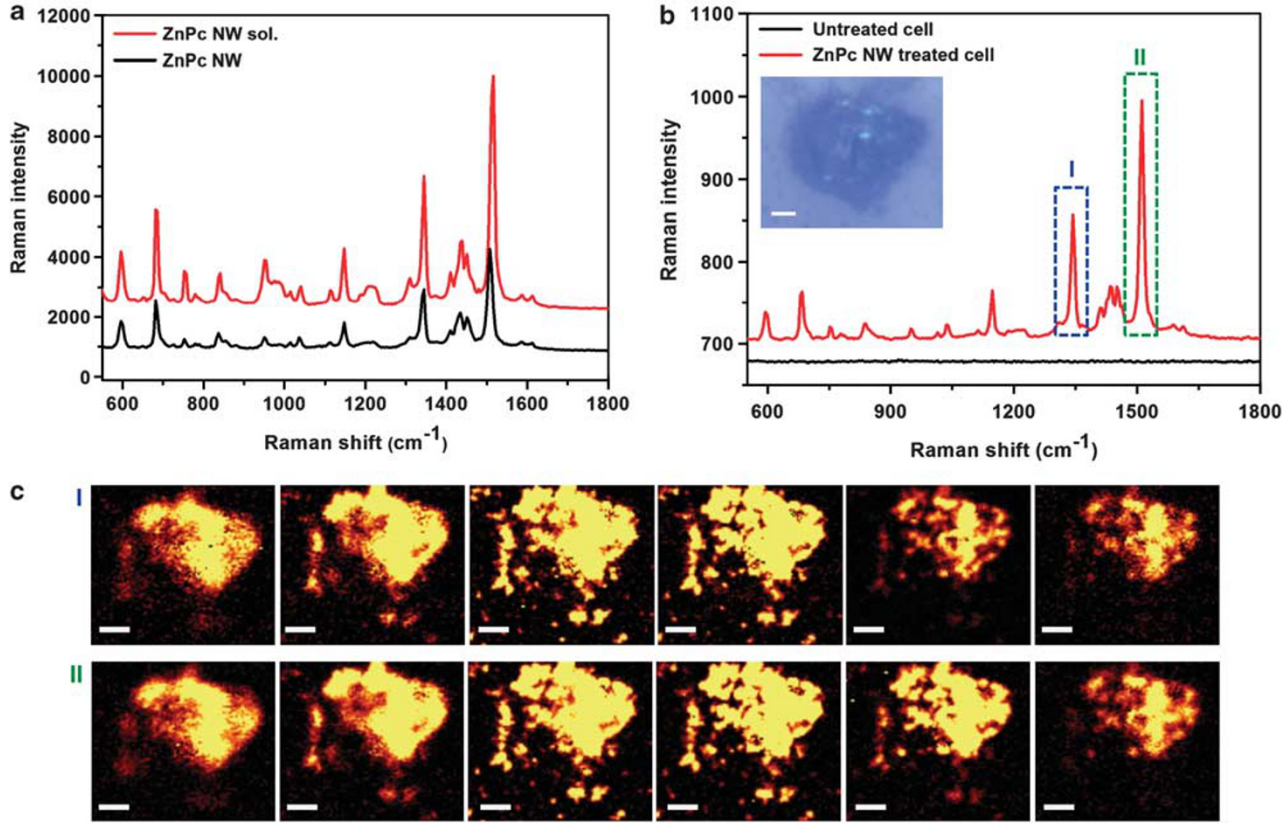

Figure 4 Intracellular internalization of ZnPc NW. (**a**) Raman spectra of ZnPc NW grown on Si substrate (black line) and ZnPc NW aqueous solution (red line). (**b**) Raman spectra from original KB cells (black line) and from KB cells treated with ZnPc NW solution (red line). The characteristic Raman features (1336 and 1506 cm^{-1}) corresponding to the pyrrole stretching mode of ZnPc are indicated by (**a**) and (**b**). (Inset) Optical microscope image of a glass plate on which KB cells treated with ZnPc NW solution are placed. The scale bar is 4 μm. (**c**) Confocal spectral images mapped with the peak intensities of I and II in (**b**). The vertical scan step (depth) is 2 μm. The color brightness depends on the peak intensity. The scale bar is 4 μm.

cells in ZnPc NW solution (50 mg l^{-1}) for 12 h, the cells show both pyrrole stretching bands, although both bands are completely absent from the untreated cell (Figure 4b). The confocal spectral images mapped with both bands (I and II in Figure 4c) confirm that ZnPc NWs are not adsorbed on the cell surface, but certainly uptaken into the cell (Figure 4c).

The synergic phototherapeutic effect of ZnPc NW on cancer-cell destruction was studied by measuring the cell viability using a colorimetric MTS assay. Although the untreated and only ZnPc NW-treated cells show high viability (Figure 5a top), the cells treated with ZnPc NWs followed by NIR ($\lambda = 808$ nm) illumination are stained with trypan blue indicating cell destruction (Figure 5a bottom left). After 24 h of the treatment, the cell destruction is more obvious (Figure 5a bottom right). Note that the cells treated with ZnPc NW and NIR initially generate some bubbles around the cell surface (Figure 5a bottom left). This phenomenon implies that cells are oxidatively damaged, which is similar to the case when the cells are treated with H_2O_2 (data not shown). The statistical data indicates that the viability of the cells treated with ZnPc NW and NIR decreases more than 50% compared with the untreated one, which is lower than other parallel sets of control groups, including the cells treated with $ZnPcS_4$ and NIR (Figure 5b).

On the basis of the *in vitro* experiment results, we performed *in vivo* experiments to evaluate phototherapeutic efficacy of ZnPc NW using a tumor-bearing mouse model. The experimental setup is shown in Figure 5c. When the tumor size reached approximately 70 mm^3 (Figure 5c top), ZnPc NW solution was introduced to the tumor region via intratumoral injection, then immediately illuminated with the same NIR laser (808 nm) at a power density of 3 W cm^{-2} for 3 min (Figure 5c middle). Figure 5d shows the tumor growth rates measured from different treatment groups. It is remarkable that the solid tumor is completely eradicated from the mouse treated with both ZnPc NW and NIR (Figure 5c bottom and Figure 5d triangle), whereas all other control groups show continuous growth of tumor. The reliability of the phototherapeutic effect of ZnPc NW was confirmed by observing similar reproducible results from four different batches. The damage to tumor tissue was further confirmed by histological assessment. The hematoxylin and eosin staining results reveal the characteristics of dead cells, such as cell shrinkages, nucleus loss and considerable karyolysis[41] in the tumor tissue treated with ZnPc NW and NIR (Supplementary Figure S12a). Moreover, a TUNEL assay, identifying necrotic or apoptotic cells, exhibits obvious brown color from most parts of the cell treated with ZnPc NW and NIR, which indicates extensive cell death (Supplementary Figure S12e). On the other hand, other control groups show robust and viable tumor cells remained (Supplementary Figures S12 b-d, f-h).

In summary, the one-dimensional ZnPc NWs grown from ZnPc PWs by the VCR process have α-form crystal structure, and exhibit substantially increased dispersibility in water. The increased

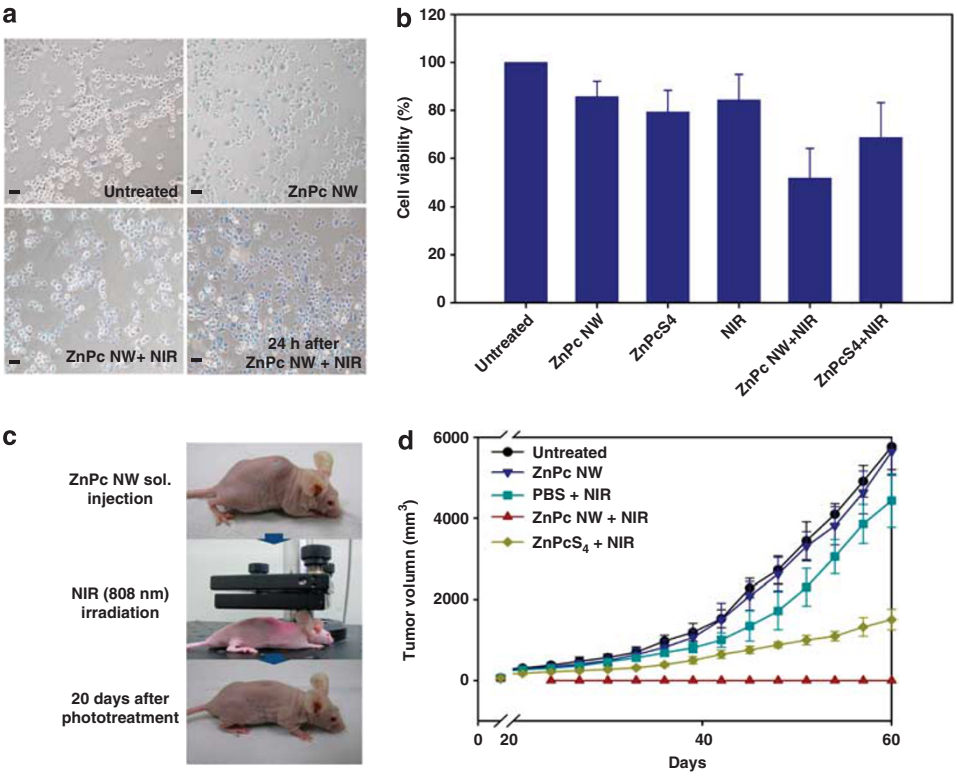

Figure 5 Synergic phototherapy of cancer using ZnPc NW. (**a**) Bright-field microscopy images of KB cells. (Top left) Untreated, (top right) treated with ZnPc NW solution (120 mg/L), (bottom left) treated with ZnPc NW solution (120 mg/L) followed by irradiation with NIR (808 nm, 3 W cm^{-2}), (bottom right) 24 h after phototreatment. The cells are stained with trypan blue, and the dead cells are observed in blue. The scale bar is 4 μm. (**b**) Quantified KB cell viability from various groups. Data are expressed as mean ± s.d. ($n = 3$, triplicate). (**c**) Photographs of *in vivo* phototherapy experiments. (Top) Mouse xenografted with KB tumor cells (tumor size is ca. 70 mm^3). (Middle) Irradiation with NIR (808 nm, 3 W cm^{-2}) on to the tumor region where ZnPc NW solution (120 mg l^{-1}, 200 μl) is intratumorally injected. (Bottom) Twenty days after phototreatment: the mouse is healthy and not showing any abnormal behaviors. (**d**) The average tumor volume is plotted against time. The tumor volume is recorded three times a week. Data are expressed as mean ± s.d. ($n = 4$, quadruplicate). Only the group treated with both ZnPc NW + NIR shows significant inhibition of tumor growth compared with untreated, ZnPc NW, PBS + NIR group ($n = 4$, $P < 0.05$, two-way ANOVA).

dispersibility of α-ZnPc NW attributes to its crystal structure providing increased chances for water to interact more with ZnPc NW over β-form ZnPc PW through hydrogen bonding (H of water to N) and coordination of water (water to Zn(II)). Although the original ZnPc photosensitizer has only a PD property, ZnPc NW exhibits dual PD and PT properties, as both *in vitro* and *in vivo* phototherapeutic experiments against KB cancer cells demonstrate successful eradication of cancer cells. We believe that our results will open a new strategy on designing the next generation photosensitizers for cancer phototherapy.

ACKNOWLEDGEMENTS

This work was supported by the National Research Foundation of Korea (NRF) grant funded by MEST (2010–0008208, 2010–0029649, 2010–0029711, 2010–00285), KOSEF through EPB center (2010–001779). HCC thanks the World Class University (WCU) program (R31-2008-000-10 059-0). XPS: 8A1 beamline of the Pohang Accelerator Laboratory (PAL) at POSTECH. We are thankful to H K Chang for technical support of hematoxylin and eosin staining and TUNEL assay in Kosin University College of Medicine.

1 Dolmans, D. E. J. G. J., Fukumura, D. & Jain, R. K. Photodynamic therapy for cancer. *Nat. Rev. Cancer* **3,** 380–387 (2003).
2 Oleinick, N. L., Morris, R. L. & Belichenko, I. The role of apoptosis in response to phtodynamic therapy: what, where, why, and how. *Photochem. Photobiol. Sci.* **1,** 1–21 (2002).
3 O'Connor, A. E., Gallagher, W. M. & Byrne, A. T. Porphyrin and nonporphyrin photosensitizers in oncology: preclinical and clinical advances in photodynamic therapy. *Phtochem. Photobiol.* **85,** 1053–1074 (2009).
4 Josefsen, L. B. & Boyle, R. W. Photodynamic therapy and the development of metal-based photosensitisers. *Met. Based Drugs* 276109–276132 (2008).
5 Triesscheijn, M., Baas, P., Schellens, J. H. M. & Stewart, F. A. Photodynamic therapy in oncology. *Oncologist* **11,** 1034–1044 (2006).
6 Juzeniene, A., Peng, Q. & Moan, J. Milestones in the development of photodynamic therapy and fluorescence diagnosis. *Photochem. Photobiol. Sci.* **6,** 1234–1245 (2007).
7 Allen, C. M., Sharman, W. M. & Lier, J. E. V. A. N. Current status of phthalocyanines in the photodynamic therapy of cancer. *Porphyr. Phthalocyanines* **5,** 161–169 (2001).
8 Owens, J. W., Smith, R., Robinson, M. & Robins, M. Photophysical properties of porphyrins, phthalocyanines and benzochlorins. *Inorg. Chem. Acta* **279,** 226–231 (1998).
9 Dhami, S. & Phillips, D. Comparison of the photophysics of an aggregating and non-aggregating aluminium phthalocyanine system incorporated into unilamellar vesicles. *J. Photochem. Photobiol. A* **100,** 77–84 (1996).
10 Ribeiro, A. O., Tome, J. P. C., Neves, M. P. M. S., Tome, A. C., Cavaleiro, J. A., Iamamoto, Y. & Torres, T. [1,2,3,4-Tetrakis(α/β-d-galactopyranos-6-yl) phthalocyaninato] zinc(II): a water-soluble phthalocyanine. *Tetrahedron Lett.* **47,** 9177–9180 (2006).
11 Atilla, D., Saydan, N., Durmus, M., Gurek, A. G., Khan, T., Ruck, A., Walt, H., Nyokong, T & Ahsen, V Synthesis and photodynamic potential of tetra- and octa-triethyleneoxysulfonyl substituted zinc phthalocyanines. *J. Photochem. Photobiol. A* **186,** 298–307 (2007).
12 Maranho, D. S., Lima, R. G., Primo, F. L., Silva, R. S. & Tedesco, A. C. Photoinducednitiric oxide and singlet oxygen release from ZnPc liposome vehicle associated with thenitrosyl ruthenium complex: synergistic effects in photodynamic therapy application. *Photochem. Photobiol.* **85,** 705–713 (2008).
13 Primo, F., Rodrigues, M. M. A., Simioni, A. R., Bentley, M. V. L. B., Morais, P. C. & Tedesco, A. C. In vitro studies of cutaneous retention of magnetic nanoemulsion loaded with zinc phthalocyanine for synergic use in skin cancer treatment. *J. Magn. Magn. Mater.* **320,** e211–e214 (2008).
14 Chatterjee, D. K., Fong, L. S. & Zhang, Y. Nanoparticles in photodynamic therapy: an emerging paradigm.. *Adv. Drug Deliver Rev.* **60,** 1627–1637 (2008).
15 Ogunsipe, A., Chen, J.-Y. & Nyokong, T. Photophysical and photochemical studies of zinc. *New J. Chem.* **28,** 822–827 (2004).
16 Yoon, S. M., Hwang, I.-C., Shin, N., Ahn, D., Lee, S. J., Lee, J. Y. & Choi, H. C Vaporization-condensation-recrystallization process-mediated synthesis of helical m-aminobenzoic acid nanobelts. *Langmuir* **23,** 11875–11882 (2007).
17 Shin, H. S., Yoon, S. M., Tang, Q., Chon, B., Joo, T. & Choi, H. C. Highly selective synthesis of C60 disks on graphite substrate by a vapor-solid process. *Angew. Chem. Int. Ed.* **47,** 693–696 (2008).
18 Yoon, S. M., Hwang, I. C., Kim, K. S. & Choi, H. C. Synthesis of single-crystal tetra(4-phyridyl)porphyrin rectangular nanotubes in the vapor phase. *Angew. Chem. Int. Ed.* **48,** 2506–2509 (2009).
19 Yoon, S. M., Lee, J., Je, J. H., Choi, H. C. & Yoon, M. Optical waveguiding and lasing action in porphyrin rectangular microtube with subwavelength wall thicknesses. *ACS Nano* **5,** 2923–2929 (2011).
20 Iwatsu, F. Crystal behavior of zinc phthalocyanine films in alchols. *J. Cryst. Growth* **71,** 629–638 (1985).
21 Iwatsu, F., Kobayashi, T. & Uyeda, N. Solvent effects on crystal growth and transformation of zinc phthalocyanine. *J. Phys. Chem.* **84,** 3223–3230 (1980).
22 Senthilarasu, S., Hahn, Y. B. & Lee, S.-H. Structural analysis of zinc phthalocyanine (ZnPc) thin films: X-ray diffraction study. *J. Appl. Phys.* **102,** 043512–043516 (2007).
23 Senthilarasu, S., Velumani, S., Sathyamoorthy, R., Subbarayan, A., Ascencio, J. A., Canizal, G., Sebastian, P. J., Chavez, J. A. & Perez, R. Characterization of zinc phthalocyanine (ZnPc) for photovoltaic applications. *Appl. Phys. A* **77,** 383–389 (2003).
24 Zeyada, H. M. & El-Nahass, M. M. Electrical properties and dielectric relaxation of thermally evaporated zinc phthalocyanine thin films. *Appl. Surf. Sci.* **254,** 1852–1858 (2008).
25 Maggioni, G., Quaranta, A., Carturan, S., Patelli, A., Tonezzer, M., Ceccato, R. & Mea, G.D. Deposition of copper phthalocyanine films by glow-discharge-induced sublimation. *Chem. Mater.* **17,** 1895–1904 (2005).
26 Saini, G. S. S., Singh, S., Kaur, S., Kumar, R., Sathe, V. & Tripathi, S. K. Zinc phthalocyanine thin film and chemical analyte interaction studies by density functional theory and vibrational techniques. *J. Phys. Condens. Matter* **21,** 225006–225015 (2009).
27 Kobayashi, T., Fujiyoshi, Y., Iwatsu, F., Uyeda, N. & High-resolution, TEM Images of zinc phthalocyanine polymorphs in thin films. *Acta Crystallogr.* **A37,** 692–697 (1981).
28 Xiao, K., Li, R., Tao, J., Payzant, E. A., Ivanov, I. N., Puretzky, A. A., Hu, W. & Geohegan, D. B. Metastable copper-phthalocyanine single-crystal nanowires and their use in fabricating high-performance field-effect transistors. *Adv. Funct. Mater.* **19,** 3776–3780 (2009).
29 Guo, Z., Chen, B., Zhang, M., Mu, J., Shao, C. & Liu, Y. Zinc phthalocyanine hierarchical nanostructure with hollow interior space: solvent-thermal synthesis and high visiblephotocatalytic property. *J. Colloid. Interface Sci.* **348,** 37–42 (2010).
30 Stymne, B., Sauvage, F. X. & Wettermark, G. A spectroscopic study of the complexation of ethanol and phenol. *Spectrochim. Acta* **35,** 1195–1201 (1979).
31 Marchon, B., Carrazza, J., Heinemann, H. & Somorjai, G. A. TPD and XPS studies of O_2, CO_2, and H_2O adsorption on clean polycrystalline graphite. *Carbon* **26,** 507–514 (1988).
32 Chiba, K., Ohmori, R., Tanigawa, H., Yoneoka, T. & Tanaka, S. H_2O trapping on various materials studied by AFM and XPS. *Fusion Eng. Des.* **49,** 791–797 (2000).
33 Cui, L.-Y., Yang, J., Fu, Q., Zhao, B.-Z., Tian, L. & Yu, H.-L. Synthesis, crystal structureand characterization of a new zinc phthalocyanine complex. *J. Mol. Struct.* **827,** 149–154 (2007).
34 Soldatova, A. V., Kim, J., Peng, X., Rosa, A., Ricciardi, G., Kenney, M. E. & Rodgers, M. A. J. Effects of benzoannulation and alpha-octabutoxy substitution on the photophysical behavior of nickel phthalocyanines: a combined experimental and DFT/TDDFT study. *Inorg. Chem.* **46,** 2080–2093 (2007).
35 Zhang, M., Murakami, T., Ajima, K., Tsuchida, K., Sandanayaka, A. S. D., Ito, O., Iijima, S. & Yudasaka, M. Fabrication of ZnPc/protein nanohorns for double photodynamic and hyperthermic cancer phototherapy. *Proc. Natl Acad. Sci. USA* **105,** 14773–14778 (2008).
36 Kuo, W.-S., Chang, C.-N., Chang, Y.-T., Yang, M.-H., Chien, Y.-H., Chen, S.-J. & Yeh, C.-S. Gold nanorods in photodynamic therapy, as hyperthermia agents and in near-infrared optical imaging. *Angew. Chem. Int. Ed.* **49,** 2711–2715 (2010).
37 Braydich-Stolle, L. K., Lucas, B., Schrand, A., Murdock, R. C., Lee, T., Schlager, J. J., Hussain, S. M. & Hofmann, M.-C. Silver nanoparticles disrupt GDNF/Fyn kinase signaling in spermatogonial stem cells. *Toxicol. Sci.* **116,** 577–589 (2010).
38 Weissleder., R. A clearer vision for *in vivo* imaging. *Nat. Biotech.* **19,** 316 (2001).
39 Sternlicht, H., Nieman, G. C. & Robinson., G. W. Triplet-triplet annihilation and delayed fluorescence in molecular aggregates. *J. Chem. Phys.* **38,** 1326–1335 (1963).
40 Palys, B. J., Puppels, G. J., van den Ham, D. & Feil, D. Raman spectra of zinc phthalocyanine monolayers adsorbed on glassy carbon and gold electrodes by application of a confocal Raman microspectrometer. *J. Electroanal. Chem.* **326,** 105–112 (1992).
41 Majno, G. & Joris, I. Apoptosis, oncosis, and necrosis an overview of cell death. *Am. J.Pathol.* **146,** 3–15 (1995).

Supplementary Information accompanies the paper on the NPG Asia Materials website (http://www.nature.com/am)